Computer simulation of elastic constants of hydroxyapatite and fluorapatite

E. Menéndez-Proupin[a], S. Cervantes-Rodríguez[b], R. Osorio-Pulgar[a], M. Franco-Cisterna[a], H. Camacho-Montes[c], and M. E. Fuentes[b,*]

[a]*Departamento de Física, Facultad de Ciencias, Universidad de Chile, Las Palmeras 3425, 780-0024 Ñuñoa, Santiago, Chile*

[b]*Laboratorio de Química Computacional, Universidad Autónoma de Chihuahua, Campus Universitario II, 31125 Chihuahua, Mexico*

[c]*Basic Science Department, IIT, Universidad Autónoma de Ciudad Juarez, Av. Del Charro 460 norte Cd. Juarez, 32310 Chihuahua, Mexico*

Date: March 1, 2011

Published at Journal of the Mechanical Behavior of Biomedical Materials **4**, 1011-1020 (2011)
Get the published version at http://dx.doi.org/10.1016/j.jmbbm.2011.03.001

*Corresponding author. Tel.: +52 614 1788201
E-mail address: mfuentes@uach.mx

Abstract

Hydroxyapatite (HAP) and fluorapatite(FAP) are essential components of dental enamel and bone. In this paper we report a computational study of the elastic properties of HAP and FAP using ab initio and forcefield techniques. We have obtained the HAP and FAP elastic stiffness constants in hexagonal symmetry by fitting the Hooke law for both the energy-strain and stress-strain relations. Our ab initio HAP stiffness constants differ from previous calculations, but follow similar trends. The HAP and FAP stiffness constants calculated with the ab initio method are very similar, although FAP is slightly stiffer than HAP in the hexagonal plane, and more compliant along the hexagonal axis. The pseudo single-crystal HAP experimental stiffness constants in current use are critically reviewed. Combining the data from the ab initio simulations with the experimental FAP stiffness constants, several alternative sets of HAP stiffness constants are proposed. The properties mismatch between HAP and FAP is evidently too small to assume it directly responsible for the dental enamel mechanical degradation with fluorosis desease.

Keywords: Hydroxyapatite; Fluorapatite; Computer simulation; Stiffness constants.

1. Introduction

Dental enamel is made up of apatitic mineralites (95-96 wt,%), organic matter (1 wt %) and water (3 wt %) (Cuy, 2002). The majority of mineralized weaves needs multiscale modeling. Detailed composition and accurate structure-property relationships of apatitic mineralites are critically important for evaluating the mechanical properties of dental enamel. According to Baldazarri (2008), small differences in material composition can lead to significant changes in their mechanical properties. Among the most important crystals that conform dental enamel are hydroxyapatites (HAP) and fluorapatites (FAP) with two formula units $Ca_5(PO_4)_3(OH,F)$ per crystal cell. Modeling the mechanical properties of these compounds using electronic structure methods entails a description on atomic scale

of some characteristics of the healthy and fluorated tooth.

This study is motivated by the question about the influence of the composition of the dental enamel on its mechanical properties. Topic fluoridation promotes ionic interchange in the external surface of HAP (non prismatic enamel) that naturally exists on top of the enamel, converting it into hypermineralized surface of FAP (De Leeuw, 2002; Ten Cate, 1999). The demineralization-remineralization process that is enhanced through this mechanism is a worldwide exploited anti-caries technique.

This must not be confused with dental fluorosis, a disease mostly related to ingestion of water with excess of fluoride. Although the existence of FAP crystals in the enamel internal tissue is not discarded in this cases, systemic fluoride mostly affects dental amelogenesis process and does not provide a real anti caries protection (Aoba and Fejerskov, 2002). As a consequence there are morphology, texture and mineral/organic matrix proportion changes that could be related to mechanical breakdown of fluorotic teeth, but they are not directly related to the atomic composition of the crystals.

The HAP crystal is mostly reported as a complex structure with 44 atoms in the hexagonal primitive cell (Chakraborty, 2006; Renaudin, 2008; Sänger and Kuhs, 1992), space group $P6_3/m$ and a 50% partial occupancy of the OH sites. It is schematically represented in Figure 1. It is also found in the monoclinic space group $P2_1/b$, depending on the stoichiometry, temperature, and synthesis pressure (Snyders, 2007; Suetsugu, 2001; Suetsugu and Tanaka, 2002). Other subgroups of $P6_3/m$, i.e., $P2_1$ and $P6_3$, have been proposed based on computational simulations (Haverty, 2005; Tofail, 2005). The differences between the different models are related with the local ordering of the OH^- groups and small distortion of the phospate tetrahedra. A triclinic structure is also reported, being a small distortion from the $P6_3/m$ structure (Alberius, 2001).

Figure 1 should be in this place

FAP has a very similar structure with 42 atoms in the same space group and no partial occupancy (F^- anions instead of OH^- groups). Calcium ions in apatite structure are in two different locations, Ca (1)

and Ca (2). The Ca (1), four by unit cell, are located far from the hexagonal axis that contains the F^- or OH^- groups and are surrounded by 6 atoms of oxygen. The Ca (2), six by unit cell, are surrounding the channels of fluoride and hydroxyl groups in groups of 3 at different heights (Hughes, 1989).

Yoon and Newnham (1969), and Sha et al. (1994) measured the elastic stiffness constants of single crystal FAP by means of ultrasonic techniques. Teraoka et al. (1998) measured bending strength and Young's modulus of HAP single crystals. To our knowledge, there are no direct experimental reports of all the components of the stiffness tensor in HAP monocrystals that form dental enamel. Katz and Ukraincik (1971) performed an extended experimental analysis of FAP single crystals to derive a set of pseudo single crystal stiffness constants for HAP. Remarkably, the values determined in (Katz and Ukraincik, 1971) constitute the only approximation to "experimental" stiffness constants available today for HAP. Recently, Tofail et al. (2009) have measured the elastic constants of a textured sample policrystalline sample of HAP that has transverse isotropy. As a transversely isotropic medium has the same number of independent elastic constants as an hexagonal crystal, the monocrystal elastic constants can be derived from the polycrystal constants, although are needed some assumptions about how the monocrystal constants are averaged over the polycrystal (see the discussion and the appendix below).

There has been recent computational efforts devoted to the mechanical properties of this material (Ching et al., 2009; De Leeuw et al., 2007; Mostafa and Brown, 2007; Snyders, 2007). In (De Leeuw et al., 2007; Mostafa and Brown, 2007) different force fields for the modeling of HAP and FAP were established based upon transferable potentials. The potentials were also used to calculate the compressibility data of HAP and FAP. Parameter free ab initio calculations have been reported for HAP (Ching et al., 2009; Snyders, 2007), using Density Functional Theory (DFT). However, the ab initio stiffness constants obtained in these calculations present significant divergence.

In this article, we calculate the stiffness constants of HAP and FAP using DFT, and analyze the results in comparison with other DFT and forcefield calculations. In Sect. 2, we describe the structural models

and the computational details. In Sect. 3, we present our results. In Sect. 4, we analyze the assumptions of (Katz and Ukraincik, 1971) and present new possible sets of stiffness constants for HAP. We also compare the properties of FAP and HAP. Sect. 5 is devoted to our conclusions.

2. Computational methods

2.1 Structural models

We studied the crystallographic structure of HAP refined by Hughes et al. (1989), as was modified by Mostafa and Brown (2007). The structure of Hughes et al., belongs to the $P6_3/m$ space group, with fractional occupations 0.5 for the OH groups. Mostafa and Brown expressed it in the P1 group and removed half of the OH groups. In fact, this structure has $P6_3$ symmetry.

The structure of FAP was taken from the experimental data in (Hughes, 1989), already used as starting structures in other computational studies (Mostafa and Brown, 2007; Tamm and Peld, 2006). It belongs to $P6_3/m$ space groups with 42 atoms per unit cell. HAP also can be constructed similarly to FAP, substituting F atoms by the OH group.

Calderin et al. (2003) reported an electronic structure calculation of HAP. They obtained that the most stable HAP structure has the OH oriented in the same direction. They also simulated double unit cells with the hexagonal *b* cell doubled along the *b* direction, and found that the OH^- groups in neighbor cells can be parallel (hexagonal crystal) or antiparallel (monoclinic crystal), indistinguishible in terms of the total energy.

2.2 Elastic properties

The elastic stiffness constants are defined as

$$C_{ij} \equiv c_{\alpha\beta\gamma\delta} = \frac{1}{\Omega}\frac{\partial^2 E_{total}}{\partial\varepsilon_{\alpha\beta}\partial\varepsilon_{\gamma\delta}}, \qquad (1)$$

where $U=E_{total}/\Omega$ is the total energy per unit volume, while $\sigma_{\alpha\beta}$ and $\varepsilon_{\alpha\beta}$ ($\alpha,\beta=x,y,z$) are the components of the stress and strain tensors, respectively. In the context of ab initio calculations, Ω is the unit cell volume, and E_{total} is the unit cell energy. The matrix of stiffness constants $C_{ij} = c_{\alpha\beta\gamma\delta}$, is defined by means of the Voigt compound indices $i=\alpha\beta$, $j=\gamma\delta$, following with the rule 1=*xx,* 2=*yy,* 3=*zz,* 4=*yz,* 5=*zx,* 6=*xy*. Due to the symmetry of hexagonal crystals, the matrix of stiffness constants of HAP and FAP can be expressed in terms of five independent constants (Dieulesaint and Royer, 1980)

$$C = \begin{pmatrix} C_{11} & C_{12} & C_{13} & 0 & 0 & 0 \\ C_{12} & C_{11} & C_{13} & 0 & 0 & 0 \\ C_{13} & C_{13} & C_{33} & 0 & 0 & 0 \\ 0 & 0 & 0 & C_{44} & 0 & 0 \\ 0 & 0 & 0 & 0 & C_{44} & 0 \\ 0 & 0 & 0 & 0 & 0 & \dfrac{(C_{11}-C_{12})}{2} \end{pmatrix} \tag{2}$$

The elastic properties can be characterized equivalently by the matrix of compliance constants S_{ij}, which is the inverse of the C matrix. The stress and strain tensors are symmetric, having only six independent components. This allows the Voigt notation, where the stress and the strain are expressed as 6x1 matrices or their transposes

$$\begin{aligned} S^T &= (\sigma_{xx} \quad \sigma_{yy} \quad \sigma_{zz} \quad \sigma_{yz} \quad \sigma_{zx} \quad \sigma_{xy}), \\ E^T &= (\varepsilon_{xx} \quad \varepsilon_{yy} \quad \varepsilon_{zz} \quad 2\varepsilon_{yz} \quad 2\varepsilon_{zx} \quad 2\varepsilon_{xy}). \end{aligned} \tag{3}$$

In the limit of infinitesimal deformation, the relationship between strain, stress and energy can be expressed in matrix notation as

$$S = CE, \qquad U = \frac{E_{total}}{\Omega} = \frac{1}{2} E^T C E. \tag{4}$$

We used the periodic DFT method to calculate energies and stress tensors of the HAP and FAP crystals subjected to strain. We applied five independent strains and fitted the stiffness constants to the energy-

strain relations, as detailed in Table I. For each type of strain, we calculated the total energies (E_{total}) for the values $\varepsilon_{\alpha\beta}$=0, ±0.0025, ±0.005, ±0.075, ±0.010, and ±0.015. The dependences $E_{total}(\varepsilon_{\alpha\beta})$ were fitted to polynomials of the kind

$$E_{total}(\varepsilon) = \Omega U(\varepsilon) = A_0 + A_1\varepsilon + A_2\varepsilon^2 + A_3\varepsilon^3. \quad (5)$$

The linear and cubic terms were necessary only in a few cases. A_1 corrects inaccuracies in the variable cell optimization, and A_3 corrects for anharmonic terms. The term A_2 was nonsensitive to the values of A_1, but the quality of the fit was improved. A_2/Ω is equal to $C_{11}/2$ for strain I, $C_{11}+ C_{12}$ for strain II, etc., as in Table I.

Table I should be here

2.3 Ab initio total energy calculations

The total energy of the unit cell was calculated using the code QUANTUM ESPRESSO (Giannozzi et al., 2009), a plane waves and pseudopotential implementation of DFT (Kohanoff, 2006). In this framework, the total energy is the sum of the internuclear Coulomb repulsion and the electronic ground state energy in the field of the nuclei. The pseudopotential framework allows to calculate only the states of the valence electrons, avoiding the explicit calculation of core states. In general, pseudopotential methods provide numerical results of the same quality as all-electron calculations. The electronic energy is obtained solving the Kohn-Sham equations (Kohanoff, 2006). For the exchange and correlation interaction, we used the well known PBE functional (Perdew, 1996). For the electron-

core interaction, we used ultrasoft pseudopotentials (Vanderbilt, 1990) [1]. We used a cutoff of 60 Ry for the plane wave expansion of the wavefunctions and 360 Ry for the charge density. Let us note that 60 Ry is an extremely high cutoff when ultrasoft pseudopotentials are used, but it was needed to obtain soft energy-strain curves. The first Brillouin zone was sampled with a 3x3x4 k-points mesh centered at the Γ point and shifted half step in the z-direction. With this setup, the energy, force and pressure are converged within 2 meV/atom, 3 meV/Å and 0.4 kbar, respectively. The stress tensor in QUANTUM ESPRESSO is calculated based on the expressions derived by Nielsen and Martin (1983). This capability makes possible to obtain the stiffness constants from the stress-strain relation (see Table I). The elastic constants obtained from the stress-strain and energy-strain relations generally differ a little due to numerical issues, but these differences can be controlled by the convergence parameters mentioned above. Hence, comparing the values obtained by both methods allows to asses the quality of the calculations.

Optimized (unstressed) structures were obtained using the variable-cell Parrinello-Rahman damped dynamics (Parrinello and Rahman, 1980), iterating until all the components of the stress tensor were smaller than 0.1 kbar, the total energy difference with the previous iteration was smaller than 1.4×10^{-5} eV (10^{-6} Ry), and the forces were smaller than 0.026 eV/Å (10^{-3} Ry/bohr). In the calculations to obtain the energy of the strained crystals, the atom positions were relaxed, using the same force and energy criteria as in the variable cell relaxations, and the BFGS algorithm implemented in QUANTUM ESPRESSO.

3. Results

[1] We have used the pseudopotentials H.pbe-rrkjus.UPF, O.pbe-rrkjus.UPF, Ca.pbe-nsp-van.UPF, and P.pbe-n-van.UPF, from the QUANTUM ESPRESSO web site http://www.quantum-espresso.org.

3.1 Relaxed structures

Table II shows the crystallographic and theoretical lattice parameters. The HAP theoretical unit cell volume is 3.6% larger than the experimental reference, in agreement with the known trend of GGA predicting larger volumes than the experiments. The theoretical volume of FAP unit cell is 2.7% larger than the crystallographic FAP structure in (Hughes, 1989).

Table II should be here

3.2 Elastic constants

Figure 2 shows the ab initio energy-strain data and the fitted curves for HAP. It can be observed a well defined relaxed structure energy minimum. Similar pictures are obtained for the cases of FAP. The stiffness constants obtained from the fits are listed in Table III and IV. The fit is qualitatively very good, and this quality is reflected in the low estimated errors of the fitted constants, reported in brackets in Table III and IV. Note that we dealt with energy differences as small as 1 meV. Although the absolute total energy is not converged, the energy differences are sufficiently converged to produce soft curves. Our initial calculations with a 35 Ry cutoff, typical for ultrasoft pseudopotentials, produced reasonable, but noisy curves. In some cases the strained cells had lower energy than the relaxed unit cell. Moreover, the 60 Ry cutoff allows a substantially better agreement between the stiffness constants fitted from the energy-strain and stress-strain data.

Figure 2, Table III and IV should be here

Only few differences deserve to be mentioned between HAP and FAP. FAP structure is more energy sensitive to elongational strain (ε_{11} and ε_{33}) and in-plane shear strain (ε_{12}) than both HAP structures

resulting in higher C_{11}, C_{33} and C_{12} for FAP. The situation for the out-of-plane shear strain (ε_{13} and ε_{44}) dependence for energy is observed to be the other way around with lower C_{13} and C_{44} for FAP.

It is well known that in GGA calculations the lattice parameters are overestimated with respect to room temperature measurements. For HAP and FAP, the difference between the experiment (Hughes, 1989) and our calculation is 3.6 % and 2.7 %, respectively. The difference is basically due to the *a* and *b* vectors, the *c* vector is almost equal in experiment and theory. To evaluate the effect of the lattice vectors overestimation on the elastic constants, we have also calculated them imposing an external pressure that allows to reproduce the experimental unit cell volume.

Using classical force-fields and the General Utility Lattice Package (GULP)(Gale and Rohl, 2003), it is possible also to obtain the elastic constants by performing analytical derivatives of the energy against the strain tensor. We have explored this kind of models using the forcefields of Mostafa and Brown (2007). The elastic constants can also be obtained fitting the energy-strain curves. We used both types of calculations to check the reliability of our fitting procedure, the stiffness constants obtained by analytical derivatives and by our fitting procedure agree within 1%.

4. Discussion

Snyders et al. (2007) calculated the C_{ij} by the method of Fast et al. (1995), which is essentially our energy vs strain method. For comparison, the numerical parameters used in (Snyders, 2007) were: 495 eV cutoff, 0.01 meV SCF convergence in total energy, 7x7x7 kpoints, VASP code. Ching et al (2009) used the stress-strain relations to calculate the C_{ij} by finite differences. The stresses were obtained with VASP. However, they used stricter convergence criteria (notably a 600 eV cutoff). They obtained nine stiffness constants in total, which can be put in correspondence with the hexagonal symmetry constants using $(C_{11}+C_{22})/2 \rightarrow C_{11}$, $(C_{12}+C_{23})/2 \rightarrow C_{12}$, and $(C_{44}+C_{55})/2 \rightarrow C_{44}$.

Ching et al. (2009) C_{ij} are greater than ours, except C_{13}, and show better agreement with the values of Katz and Ukraincik (1971). However, as will be discussed below this coincidence may be fortuitous. Snyders et al. (2007) obtained smaller C_{12} and C_{13} than ours, but greater C_{33} and C_{44}, averaging a similar bulk modulus and larger shear modulus compared to our calculation. Their results for C_{33} and C_{44} are more than 40% larger than our results, and are also higher that all other calculations. They also obtained an anomalous low *c/a* ratio. It is difficult to assess the cause of the dispersion of the ab initio C_{ij} values, provided that the three calculations share common methods. The three calculations used the periodic DFT approach, with plane wave basis sets and the GGA. Snyders et al. (2007) and Ching et al. (2009), used the same code VASP; Snyders et al. used ultrasoft pseudopotentials, like us, while Ching et al. used the projector augmented wave potential. Ching et al. used the same functional than us, PBE, while Snyders et al. used a non-specified GGA functional, probably PW91 or PBE. These methodological differences generally produce marginal differences and do not explain the variability of the results. To discard errors induced by different pseudopotentials and other implentation details, we have made test calculations of the C_{ij} constants using the VASP code. For the VASP calculations we have used the set of parameters specified by Ching et al. (2009), and we have obtained the values C_{11}=123 GPa, C_{12}=34 GPa, C_{13}=66 GPa, C_{33}=168 GPa, which are rather close to numbers obtained with QUANTUM ESPRESSO. We have explored variations of the fitting procedure, the k-points grid, 44 and 88 atoms unit cells, and we have been unable to reproduce the results of Ching et al. (2009). Professor Ching has kindly supplied his refined structure with an orthorhombic unit cell, and we have obtained the same values for the elastic constants.

We have also tested a structural model with $P2_1/b$ symmetry derived from the crystallographic structure of (Sänger and Kuhs, 1992). This model has the same backbone with $P6_3/m$ symmetry, but the OH groups along the same line (*c* axis) have opposite orientations, with the hydrogens pointing toward each other. The relaxed structure has a slightly higher energy (6 meV/atom) than the above described

model. The elastic constants computed with both structures have no significant differences (less than 2.5 Gpa).

Mostafa and Brown (2007) fitted empirical forcefields to the structure and physical data of FAP, and used them to calculate the stiffness constants of HAP and FAP. Noting some errata in (Mostafa and Brown, 2007), we have recalculated the stiffness constants and written them in Table III and IV. De Leeuw et al. (2007) have also fitted forcefields to simulate a number of properties of apatites, including the elastic properties. For the sake of completeness, we include their results in Tables III, IV, and V.

Comparing the ab initio stiffness constants of HAP and FAP with the experimental values, we observe that C_{11}, C_{12} , and C_{33} are significantly smaller than the experimental ones, while C_{13} and C_{44} have larger or similar ab initio values.

The calculation with the external pressure produces higher stiffness constants except for C_{44}, which describes the response to shear stress. In the case of FAP, the pressure makes the values of C_{11}, C_{12}, and C_{33} to fall within the values of the two reported experiments. In the case of HAP under pressure, all the stiffness constants but C_{44}, are higher than the experimental values.

Van der Waals interaction, not reproduced by standard DFT (French et al, 2010), provide and additional attractive potential that contribute to reduce the unit cell volume and increase the stiffness constants. In apatites, the dominant interactions are ionic and covalent, which are several orders of magnitude stronger than van der Waals interactions. An estimation of the van der Waals effect upon the elastic properties can be obtained from force field calculations (Mkhonto and de Leeuw, 2002), where dispersion terms of the form C/r^6 are fitted for the O-O, O-F and F-F pair potentials. When the FAP elastic constants are recalculated without the dispersion potentials, the elastic constants decrease 2.2 GPa for C_{11} and C_{12} and less for the other constants. This is consistent with the known trend of van der Waals bound solids to have Young moduli in the range 1-4 GPa (Ashby et al, 2007, pag 67). Hence,

one can expect that a van der Waals corrected calculation may increase the stiffness constants in about 2 GPa.

The obtained elastic constants are typical of ionic solids (see. e.g., Catti et al (1991)). As shown by analysis of Mulliken charges and bond orders (Rulis et al, 2004), FAP and HAP have strong covalent bonding within the phosphate and hydroxyl groups and ionic bonding between Ca^{2+}, PO_4^{3-}, F^-, and OH^-. Hence, according to the mechanical behavior, they can be regarded as ionic solids with complex ions.

Let us comment on the experimental stiffness constants. Gilmore and Katz (1982) obtained values of the bulk and shear moduli of dense polycrystalline HAP and FAP, as well as enamel and dentin, by measurement of the ultrasonic velocities in compressed powders with different pressures, and extrapolation to zero pressure to filter the effect of porosity. They obtained for HAP the values B=89.0 GPa, G=44.5 GPa, E=114 GPa. For FAP, B=94.0 GPa, G=46.4 GPa, and E=120 GPa. The Young modulus is calculated as $E=9BG/(3B+G)$. They also showed that for composites HAP-NaCl, the Reuss approximation performs better than the Voigt's one.

The experimental data reported by Yoon and Newnham (1969), and by Sha et al. (1994) for FAP provide the only experimental values of the elastic constants of fluorapatite to date. Katz and Ukraincik (1971) assumed that the single crystal stiffnesses coefficients could be calculated for HAP by scaling the HAP isotropic moduli against the corresponding FAP moduli. They assumed that the combinations $2C_{11}+C_{33}$, $C_{12}+2C_{13}$, and $(C_{11}-C_{12})/2+2C_{44}$ have a constant ratio HAP/FAP=0.955, which is the average ratio of the measured bulk and shear moduli. These combinations appear in the Voigt averages, considering the symmetry constraints for the hexagonal group. Katz and Ukraincik also assumed that $(C_{11}+C_{12}-2C_{13})/(C_{33}-C_{13})$ and $2C_{44}/(C_{11}-C_{12})$ take the same values in both FAP and HAP crystals. Solving the equations, they determined the pseudo single crystal stiffness constants of HAP. However, the measured bulk modulus in both FAP and HAP are inconsistent with the Voigt bulk moduli

determined from the single crystal stiffness constants. In fact, they are out of the range between Reuss and Voigt values. Moreover, Table V shows the HAP/FAP ratios of the combinations of the stiffness constants used in (Katz and Ukraincik, 1971), and the values obtained from simulations with ab initio and forcefield models. It can be seen that some of the ratios deviate considerably from the values assumed in (Katz and Ukraincik, 1971). Finally, using the ratios given by the simulations, we have recalculated the HAP stifness constants with the method of Katz and Ukraincik (1971) and present them in Table V.

Table V should be here

Just recently, Tofail et al. (2009) have measured the elastic constants of a textured sample of HAP, such that the hexagonal axes of the grains are aligned in the XY plane of the sample, and arbitrarily oriented within this plane. This sample had transverse isotropic symmetry. The elastic constants of the textured material can be estimated by averages of the stiffness tensor (Voigt averages) and by averages of the compliance tensor (Reuss averages), as discussed in the Appendix. As the transversely isotropic medium has the same number of independent elastic constants as the hexagonal crystal, the above equations can be easily solved to obtain the monocrystal stiffness constants from the policristal constants. Table III shows the monocrystal stiffness constants derived from the polycrystal constants assuming the Voigt and Reuss conditions. Comparison between estimated monocrystal properties and Katz and Ukraincik data shows a somewhat unexpected disagreement, also showing the scattering of the experimental data in the literature due to difficulties to obtain accurate measurements. The newly derived C_{11} is smaller than the Katz and Ukraincik values and closer to the ab initio value. C_{33} is also smaller than Katz and Ukraincik values, with the DFT values in between. C_{12} and C_{44} are higher than both other values. C_{13} is between the DFT and Katz and Ukraincik values.

In all the experimental and theoretical results the differences between corresponding C_{ij} values and unit cell parameters of HAP and FAP are too small to entail any dramatical change in tooth mechanical properties. They don't seem to be directly responsible of mechanical breakdowns in enamel with fluorosis. In accordance with Baldazarri et al. (2008) results, the existence of residual organic matrix in dental enamel seems a most important factor because of mechanical mismatch between ceramics and organic materials. Nevertheless, the question about the influence of morphology and texture of polycrystalline structures remains open. Although hyper-mineralized enamel surfaces containing large amounts of FAP could be more rigid than purely HAP compositions, regarding this is a general tendency verified by all the cited methods.

5. Conclusions

We have presented a first principles calculation of the elastic stiffness constants of FAP and HAP. We have studied the effect of the HAP alternative structures on the stiffness constants. We have discussed the dispersion of the stiffness constants calculated by different authors using similar methods. The DFT stiffness constants are, in general, significantly smaller than the experimental values, with the exception of C_{13}. Setting an empirical external pressure to reproduce the experimental unit cell density, allows to improve the elastic constants for FAP, giving values that fall between the two available experimental measures. However, in the case of HAP the external pressure does not improve the agreement with experimental values of stiffness constants. Hence, purely ab initio methodology is presently unable to predict accurate values of the HAP elastic constants (or there is a very ample range for them). Nevertheless, the experimental values of HAP elastic constants are based on measurements in polycrystalline samples and differ as much as 24%. However, DFT reproduces the experimental findings of (Sha et al., 1994) and (Yoon and Newnham, 1969) about the anisotropy, i.e., C_{33}/C_{11}. Moreover, combining the data from our ab initio calculations with the experimental FAP data, we have recalculated the HAP pseudo single crystal stiffness constants, providing updated and reasonable

values. In the new sets of HAP stiffness constants C_{13}, C_{33}, and C_{44} are larger than the old values (Katz and Ukraincik, 1971) , while and C_{11} and C_{12} are similar. We hope that our results stimulate efforts to measure precisely the single crystal elastic constants of HAP. Regarding the problem of dental enamel, the elastic properties mismatch between HAP and FAP seems to be too small to explain the degradation of mechanical properties with fluorosis disease. The influence of residual organic matrix, crystal morphology and texture can be more reasonable causes for mechanical degradation and it remains an open topic for investigation.

Appendix. Elastic constants of polycrystalline apatites

In isotropic, non textured, polycrystalline materials, there are only two independent elastic constants, such as the bulk (B) and shear (G) moduli. Other constants like Young modulus, Poisson ratio and Lamé coefficients are expressed in terms of B and G. Isotropic moduli are averages of the elastic constants of the monocrystals, but also depend on the way that individual grains interact with each other.

Two bounds average values can be easily calculated if it is assumed that the strain or the stress is continuous across grain boundaries. Assuming continuous strain one obtains the Voigt averages (Nye, 1957)

$$B_{Voigt} = \frac{1}{9}\left[C_{11} + C_{22} + C_{33} + 2\left(C_{12} + C_{13} + C_{23}\right)\right] \tag{6}$$

$$G_{Voigt} = \frac{1}{15}\left[C_{11} + C_{22} + C_{33} + 3\left(C_{44} + C_{55} + C_{66}\right) - C_{12} - C_{13} - C_{23}\right] \tag{7}$$

If the stress is assumed to be continuous across the grain boundaries, the Reuss average values follows

$$B_{Reuss} = \left[S_{11} + S_{22} + S_{33} + 2\left(S_{12} + S_{13} + S_{23}\right)\right]^{-1} \tag{8}$$

$$G_{Reuss} = 15\left[4\left(S_{11} + S_{22} + S_{33} - S_{12} - S_{13} - S_{23}\right) + 3\left(S_{44} + S_{55} + S_{66}\right)\right]^{-1} \tag{9}$$

where C_{ij} and S_{ij} are the components of the stiffness matrix defined in Eq. (1) and its inverse (i.e., the compliance matrix). The Voigt-Reuss-Hill elastic moduli are the arithmetic averages of the Voigt and Reuss values, and are considered generally a better approximation to the experimental values.

In a textured polycrystal, the function $f(\varphi,\theta,\psi)$ describes the probability to have grains with the principal crystal axes rotated with respect to reference axes, the rotation being described by Euler angles (φ,θ,ψ). The stiffness tensor of a rotated monocrystal expressed in reference axes is given as

$$c_{\alpha\beta\gamma\delta}(\varphi,\theta,\psi)=\sum_{\alpha',\beta',\gamma',\delta'=1}^{3} a_{\alpha\alpha'}a_{\beta\beta'}a_{\gamma\gamma'}a_{\delta\delta'}c_{\alpha'\beta'\gamma'\delta'},$$

where $c_{\alpha'\beta'\gamma'\delta'}$ is the tensor expressed in the principal axes of the crystal (Eq. 2), and $a_{\mu\nu}$ is the Euler rotation matrix

$$a(\varphi,\theta,\psi)=\begin{pmatrix} \cos\varphi\cos\psi-\cos\theta\sin\varphi\sin\psi & -\cos\psi\sin\varphi-\cos\theta\cos\varphi\sin\psi & \sin\theta\sin\psi \\ \cos\theta\cos\psi\sin\varphi+\cos\varphi\sin\psi & \cos\theta\cos\varphi\cos\psi-\sin\varphi\sin\psi & -\cos\psi\sin\theta \\ \sin\theta\sin\varphi & \cos\varphi\sin\theta & \cos\theta \end{pmatrix}$$

A Voigt average can be cast as

$$\left\langle c_{\alpha\beta\gamma\delta}\right\rangle_V=\int_0^{2\pi}\int_0^{\pi}\int_0^{2\pi} f(\varphi,\theta,\psi)c_{\alpha\beta\gamma\delta}(\varphi,\theta\psi)\sin\theta d\varphi d\theta d\psi$$

A Reuss average results from application of the same transformations to the compliance tensor. The standard Voigt and Reuss averages for non textured polycrystals are obtained when $f(\varphi,\theta,\psi)=1/8\pi^2$. With these transformations the stiffness and compliance tensors become isotropic and using the relations $B=(C_{11}+2C_{12})/3=1/(3S_{11}+6S_{12})$ and $G=C_{44}=1/S_{44}$, C_{ij} and S_{ij} being the averaged constants, the Eq. 6 to 9 are obtained.

For a textured sample of HAP, such that the hexagonal axes of the grains are aligned in the XY plane of the sample, and arbitrarily oriented within this plane (Tofail, 2009), we can consider $f(\varphi,\theta,\psi)=\delta(\theta-\pi/2)/4\pi^2$. This sample has transversely isotropic symmetry. The Voigt averages for this texture are

$$C_{11}^{Voigt} = \frac{1}{8}\left(3C_{11} + 2C_{13} + 3C_{33} + 4C_{44}\right)$$

$$C_{12}^{Voigt} = \frac{1}{8}\left(C_{11} + 6C_{13} + C_{33} - 4C_{44}\right)$$

$$C_{13}^{Voigt} = \frac{1}{2}\left(C_{12} + C_{13}\right)$$

$$C_{33}^{Voigt} = C_{11}$$

$$C_{44}^{Voigt} = \frac{1}{4}\left(C_{11} - C_{12} + 2C_{44}\right)$$

and the Reuss averages of the compliance constants are

$$S_{11}^{Reuss} = \frac{1}{8}\left(3S_{11} + 2S_{13} + 3S_{33} + S_{44}\right)$$

$$S_{12}^{Reuss} = \frac{1}{8}\left(S_{11} + 6S_{13} + S_{33} - S_{44}\right)$$

$$S_{13}^{Reuss} = \frac{1}{2}\left(S_{12} + S_{13}\right)$$

$$S_{33}^{Reuss} = S_{11}$$

$$S_{44}^{Reuss} = S_{11} - S_{12} + \frac{S_{44}}{2}$$

The asymmetry between the averages of C_{ij} and S_{ij} is easily understood considering their relations with the corresponding tensors, $C_{44}=c_{1212}$ vs $S_{44}=4s_{1212}$, which in turn originates in the different way that the strain and stress tensors enter in the Voigt notation, i.e., Eq. (3).

Acknowledgments

This work was supported by Programa Bicentenario de Ciencia y Tecnología (Chile) Grant No. ACT/ADI-24 and CONACYT (Mexico) Grant No. 25380 and Grant No. 100559. We also acknowledge N. Mostafa for help to reproduce its calculations, and S. Baroni for useful comments. M. E. F. is grateful to Centro Nacional de Supercómputo, IPICYT and D. Rios-Jara for invaluable computational support.

References

Alberius-Henning, P., Adolfsson, E., Grins, J., Fitch, A., 2001. Triclinic oxy-hydroxyapatite. J. Mater.

Science 36, 663-668.

Aoba, T., Fejerskov, O., 2002. Dental Fluorosis: Chemistry and Biology. Crit. Rev. Oral. Biol. Med. 13, 155-170.

Ashby, M.F., Shercliff, H., Cebon, D., 2007. Materials: engineering, science, processing and design. Butterworth-Heinemann, Oxford.

Baldazarri, M., Margolis, H.C., Beniash, E., 2008. Compositional Determinants of Mechanical Properties of Enamel. J. Dent. Res. 87, 645–649.

Calderin, L., Stott, M.J., Rubio, A., 2003. Electronic and crystallographic structure of apatites. Phys. Rev. B 67, 134106-1-7.

Catti, M., Dovesi, R., Pavese, A., Saunders, V.R., 1991. Elastic constants and electronic structure of fluorite (CaF2): an ab initio Hartree-Fock study. J. Phys.: Condens. Matter 3, 4151-4164.

Chakraborty, S., Bag, S., Pal, S., Mukherjee, A.K., 2006. Structural and microstructural characterization of bioapatites and synthetic hydroxyapatite using X-ray powder diffraction and Fourier transform infrared techniques. J. Appl. Crystallogr. 39, 385-390.

Ching, W.Y., Rulis, P., Misra, A., 2009. Ab initio elastic properties and tensile strength of crystalline hydroxyapatite. Acta. Biomater. 5, 3067-3075.

Cuy, J.L., Mann, A.B., Livi, K.J., Teaford, M.F., Weihs, T.P., 2002. Nanoindentation mapping of the mechanical properties of human molar tooth enamel. Arch. Oral. Biol. 47, 281–291.

De Leeuw, N.H., 2002. Density functional theory calculations of local ordering of hydroxy groups and fluoride ions in hydroxyapatite. Phys. Chem. Chem. Phys. 4, 3865–3871.

De Leeuw, N.H., Bowe, J.R., Rabone, J., 2007. A computational investigation of stoichiometric and calcium-deficient oxy- and hydroxy-apatites. Faraday Discuss. 134, 195–214.

Dieulesaint, E., Royer, D., 1980. Elastic Waves in Solids. Wiley, Chichester.

Fast, L., Wills, J.M., Johansson, B., Eriksson O., 1995. Elastic constants of hexagonal transition metals: Theory. Phys. Rev. B 51, 17431-17438.

French, R.H., Parsegian, V.A., Podgornik, R., Rajter, R.F., Jagota, A., Luo, J., Asthagiri, D., Chaudhury, M.K., Granick, S., Kalinin, S., Kardar, M., Kjellander, R., Langreth, D.C., Lewis, J., Lustig, S., Wesolowski, D., Wettlaufer, J.S., Ching, W.-Y., Finnis, M., Houlihan, F., von Lilienfeld, O. A., van Oss, C.J., Zemb, T., 2010. Long range interactions in nanoscale science. Rev. Mod. Phys. 82, 1887-1944.

Gale, J., Rohl, A., 2003. The General Utility Lattice Program (GULP). Mol. Simul. 29, 291-341.

Giannozzi, P., Baroni, S., Bonini, N., Calandra, M., Car, R., Cavazzoni, C., Ceresoli, D., Chiarotti, G., Cococcioni, M., Dabo, I., Dal Corso, A., de Gironcoli, S., Fabris, S., Fratesi, G., Gebauer, R., Gerstmann, U., Gougoussis, C., Kokalj, A., Lazzeri, M., Martin-Samos, L., Marzari, N., Mauri, F., Mazzarello, R., Paolini, S., Pasquarello, A., Paulatto, L., Sbraccia, C., Scandolo, S., Sclauzero, G., Seitsonen, A., Smogunov, A., Umari, P., Wentzcovitch, R., 2009. QUANTUM ESPRESSO: a modular and open-source software project for quantum simulations of materials. J. Phys. Condens. Matter. 21, 395502-1-19.

Gilmore, R.S., Katz, J.L., 1982. Elastic properties of apatites. J. Mater. Science 17, 1131-1141.

Haverty, D., Tofail, S.A.M., Stanton, K.T., McMonagle, J.B, 2005. Structure and stability of hydroxyapatite: Density functional calculation and Rietveld analysis. Phys. Rev. B 71, 094103-1-9.

Hughes, C.M., Cameron, M., Crowley, K., 1989. Structural variations in natural F, OH, and Cl apatites. Am. Mineral. 74, 870-876.

Katz, J.L., Ukraincik, K., 1971. On the anisotropic elastic properties of hydroxyapatite. J. Biomech. 4, 221-227.

Kohanoff, J., 2006. Electronic Structure Calculations for Solids and Molecules: Theory and Computational Methods, Cambridge University Press, Cambridge.

Mkhonto, D., de Leeuw, N.H., 2002. A computer modelling study of the effect of water on the surface structure and morphology of fluorapatite: introducing a $Ca_{10}(PO_4)F_2$ potential model. J. Mater. Chem. 12, 2633-2642.

Mostafa, N.Y., Brown, P.W., 2007. Computer simulation of stoichiometric hydroxyapatite: structure and substitutions. J. Phys. Chem. Solids 68, 431-437.

Nielsen, O.H., Richard, M., 1983. First-Principles Calculation of Stress. Phys. Rev. Lett. 50, 697-700.

Nye, J.F., 1957. Physical properties of crystals. Oxford University Press, New York.

Parrinello, M., Rahman, A., 1980. Crystal Structure and Pair Potentials: A Molecular-Dynamics Study. Phys. Rev. Lett. 45, 1196–1199.

Perdew, J.P., Burke, K., Ernzerhof, M., 1996. Generalized Gradient Approximation Made Simple. Phys. Rev. Lett. 77, 3865-3868.

Renaudin, G., Laquerriere, P., Filinchuk, Y., Jallot, E., Nedelec, J.M., 2008. Structural characterization of sol-gel derived Sr-substituted calcium phosphates with anti-osteoporotic and anti-inflammatory properties. J. Mater. Chem. 18, 3593-3600.

Rulis, P., Ouyang, L., Ching, W.Y., 2004. Electronic structure and bonding in calcium apatite crystals: Hydroxyapatite, fluorapatite, chlorapatite, and bromapatite. Phys. Rev. B 70, 155104.

Sänger, A.T., Kuhs, W.F., 1992. Z. Kristallogr. 199, 123-148.

Sha, M., Li, Z., Bradt, R.C., 1994. Single-crystal elastic constants of fluorapatite, $Ca_5F(PO_4)_3$. J. Appl. Phys. 75, 7784-7787.

Snyders, R., Music, D., Sigumonrong, D., Schelnberger, B., Jensen, J., Schneider, J.M., 2007. Experimental and ab initio study of the mechanical properties of hydroxyapatite. Appl. Phys. Lett. 90, 193902-1-3.

Suetsugu, Y., Ikoma, T., Tanaka, J., 2001. Single crystal growth and structure analysis of monoclinic hydroxyapatite. Key Eng. Mater. 192, 287-290.

Suetsugu, Y., Tanaka, J., 2002. Crystal growth and structure analysis of twin-free monoclinic hydroxyapatite. J. Mater. Sci.: Mater. Med. 13, 767-772.

Tamm, T., Peld, M., 2006. Computational study of catión substitutions in apatites. J. Solid State Chem. 179, 1581-1587.

Ten Cate, J.M., 1999. Current concepts on the theories of the mechanism of action of fluoride. Acta. Odontol. Scand. 57, 325-329.

Teraoka, K., Ito, A., Maekawal, K., Onuma, K., Tateishi, T., Tsutsumi, S., 1998. Mechanical Properties of Hydroxyapatite and OH-carbonated Hydroxyapatite Single Crystals. J. Dent. Res. 77, 1560-1568.

Tofail, S.A.M., Haverty, D., Stanton, K.T., McMonagle, J. B., 2005. Structural order and dielectric behaviour of hydroxyapatite. Ferroelectrics 319, 117–123.

Tofail, S.A.M., Haverty, D., Cox, F., Erhart, J., Hána, P., Ryzhenko, V., 2009. Direct and ultrasonic measurements of macroscopic piezoelectricity in sintered hydroxyapatite. J. Appl. Phys. 105, 064103-1-5.

Vanderbilt, D., 1990. Soft self-consistent pseudopotentials in a generalized eigenvalue formalism. Phys. Rev. B 41, 7892-7895.

Yoon, H.S., Newnham, R.E., 1969. Elastic properties of fluorapatite. Am. Mineral. 54, 1193-1197.

Tables

Table I. Strains, and energy-strain and stress-strain relationships used to determine the elastic constants.

Name	Non-zero strain	Energy density	Non-zero stress
I	ε_{xx}	$U=\frac{1}{2}C_{11}\varepsilon_{xx}^2$	$\sigma_{xx}=C_{11}\varepsilon_{xx},\sigma_{yy}=C_{12}\varepsilon_{xx},\sigma_{zz}=C_{13}\varepsilon_{xx}$
II	$\varepsilon_{xx}=\varepsilon_{yy}$	$U=\left(C_{11}+C_{12}\right)\varepsilon_{xx}^2$	$\sigma_{xx}=\sigma_{yy}=\left(C_{11}+C_{12}\right)\varepsilon_{xx},\sigma_{zz}=2C_{13}\varepsilon_{xx}$
III	ε_{zz}	$U=\frac{1}{2}C_{33}\varepsilon_{zz}^2$	$\sigma_{xx}=\sigma_{yy}=C_{13}\varepsilon_{zz},\sigma_{zz}=C_{33}\varepsilon_{zz}$
IV	$\varepsilon_{xx}=\varepsilon_{zz}$	$U=\frac{1}{2}\left(C_{11}+2C_{13}+C_{33}\right)\varepsilon_{xx}^2$	$\sigma_{xx}=\left(C_{11}+C_{13}\right)\varepsilon_{xx},\sigma_{yy}=\left(C_{12}+C_{13}\right)\varepsilon_{xx},$ $\sigma_{zz}=\left(C_{13}+C_{33}\right)\varepsilon_{xx}$
V	ε_{yz}	$U=2C_{44}\varepsilon_{yz}^2$	$\sigma_{yz}=2C_{44}\varepsilon_{yz}$

Table II. Crystallographic and theoretical lattice parameters of the structures of interest.

Material	a (Å)	b (Å)	c (Å)	c/a	α (º)	β (º)	γ (º)	Ω (Å^3)
			Theory					
HAP (this work)	9.582	9.580	6.879	0.72	90.00	90.00	120.00	546.85
HAP (this work) (P=29.18 kbar)	9.435	9.435	6.850	0.73	90.00	90.00	120.00	528.01
FAP (this work)	9.509	9.509	6.898	0,73	90,00	90,00	119,99	540,18
FAP (this work) (P=22.76 kbar)	9.406	9.406	6.866	0.73	90.00	90.00	120.00	526.05
HAP (Snyders, 2007)	9,635		6.595	0.68				530.20
HAP (Ching et al., 2009)	9,554		6.894	0.72				545.06
			Experiment					
HAP (Hughes, 1989)	9.418	9.416	6.875	0.73	90.01	89.99	119.94	527.99
FAP (Hughes, 1989)	9.398	9.397	6.878	0.73	89.99	90.02	120.06	526.04

Table III. HAP stiffness constants (in GPa). For each material, the constants in the first row have been fitted to the energy-strain relations. In the second row they have been fitted to the stress-strain relations. The fitting statistical error of the last digit is enclosed in brackets (two standard deviations).

	C_{11}	C_{12}	C_{13}	C_{33}	C_{44}	B^a	G^a
E vs strain	117.71(7)	31.1(1)	66.42(7)	165.0(1)	38.5(1)	77(4)	39.3(5)
Stress-strain	117.9(2)	30.55(7)	66.4(2)	165.0(2)	38.5(3)	77(4)	39.4(6)
Stress-strain (P=29.18 kbar)	145.2(3)	47.8(1)	73.6(2)	191.4(2)	37.6(8)	95(2)	43.4(5)
Forcefields (Mostafa and Brown, 2007)	158	57.5	59.8	147	43.9	90.77(3)	46.6(1)
			Others: Theory				
(Ching et al., 2009)	140.0 134.8	42.4	58.3 60.1	174,8	47.5 47.6	84.6(1.1)	47.6(1)
(Snyders, 2007)	117.1	26.2	55.6	231.8	56.4	76(6)	52(1)
(De Leeuw et al., 2007)	134.4	48.9	68.5	184.7	51.4	90(2)	46.6(4)
			Experiments				
(Katz and Ukraincik, 1971)	137	42.5	54.9	172	39.6	82.6(8)	44.6(3)
Isotropic ceramic (Gilmore and Katz, 1982)						89[b]	44.5[b]
Textured ceramics[c] (Tofail et al, 2009)	137.2	53	55.1	123.2	42.2		
Monocristal, from Voigt average[d]	123.2	51	59.2	138.8	48.3		
Monocristal, from Reuss average[d]	123.6	51.6	59.5	139.6	50.9		

[a] Voigt-Reuss-Hill (VRH) averages of bulk (B) and shear moduli (G) calculated with the stiffness constants. Shown in parentheses is the difference of the VRH average with the Voigt and Reuss values, which are theoretical upper and lower limits, respectively.

[b] Experimental values.

[c] Experimental value for a textured transversely isotropic textured polycrystal sample.

[d] Derived from the experimental values on the textured isotropic polycrystal sample. See the appendix for details.

Table IV. FAP stiffness constants (in GPa). For each material, the constants in the first row have been fitted to the energy-strain relations. In the second row they have been fitted to the stress-strain relations. The fitting statistical error of the last digit is enclosed in brackets (two standard deviations).

	C_{11}	C_{12}	C_{13}	C_{33}	C_{44}	B^a	G^a
E vs strain	126.35(9)	36.2(2)	63.4(3)	167.6(2)	34(1)	81(2)	39.2(5)
Stress-strain	126.4(8)	35.8(3)	63.0(4)	167.7(5)	35(1)	81(2)	39.8(5)
Stress-strain (P=22.76 kbar)	146.9(2)	48.4(1)	69.4(2)	188.2(2)	32(1)	94(2)	41(1)
Forcefields (Mostafa and Brown, 2007)	165	55	60	145	40.2	91.6(1)	46.6(5)
Others: Theory							
Forcefields (De Leeuw et al., 2007)	150.6	62.8	73.6	176.6	53.2	99.2(6)	47.7(2)
Experiments							
(Yoon and Newnham, 1969)	143.4	44.5	57.5	180.5	41.5	86.5(9)	46.7(3)
(Gilmore and Katz, 1982)						94[b]	46.4[b]
(Sha et al., 1994)	152.0	49.7	63.1	185.8	42.8	92.8(8)	47.9(3)

[a] Voigt-Reuss-Hill (VRH) averages of bulk (B) and shear moduli (G) calculated with the stiffness constants. Shown in parentheses is the difference of the VRH average with the Voigt and Reuss values, which are theoretical upper and lower limits, respectively.

[b] Experimental values.

Table V. Ratio of the combinations of the stiffness constants assumed in (Katz and Ukraincik, 1971) to obtain the HAP pseudo single crystal stiffness constants, compared with the values obtained from simulations. Also are given the HAP stiffness constants (in GPa) as predicted with the method of (Katz and Ukraincik, 1971) using all the above ratios and the FAP experimental values of Yoon and Newnham (1969).

	Katz and Ukraincik (1971)	DFT	Forcefields Mostafa and Brown (2007)	Forcefields de Leeuw et al (2007)
$\frac{(2C_{11}+C_{33})_{HAP}}{(2C_{11}+C_{33})_{FAP}}$	0.955	0.95	0.98	0.949
$\frac{(C_{12}+2C_{13})_{HAP}}{(C_{12}+2C_{13})_{FAP}}$	0.955	1.006	1,01	0.885
$\frac{((C_{11}-C_{12})/2+2C_{44})_{HAP}}{((C_{11}-C_{12})/2+2C_{44})_{FAP}}$	0.955	1.06	1.02	0.968
$\frac{(C_{11}+C_{12}-2C_{13})/(C_{33}-C_{13})_{HAP}}{(C_{11}+C_{12}-2C_{13})/(C_{33}-C_{13})_{FAP}}$	1.000	0.47	0.94	0.62
$\frac{2C_{44}/(C_{11}-C_{12})_{HAP}}{2C_{44}/(C_{11}-C_{12})_{FAP}}$	1.001	1.18	1.2	0.992
C_{11}	137	128[a]	137	128
C_{12}	42.5	33.6[a]	46.9	31.3
C_{13}	54.9	63.4[a]	57.2	54.9
C_{33}	172	189[a]	182	188
C_{44}	39.6	46.8[a]	45.1	40.1

[a]If the FAP stiffness constants determined by Sha et al (1994) are used together with the DFT HAP/FAP ratios, then the predicted constants are as follows: C_{11}=136 GPa, C_{12}=38.4 GPa, C_{13}=69.3 GPa, C_{33}=194 GPa, and C_{44}=48.3 GPa.

Figures

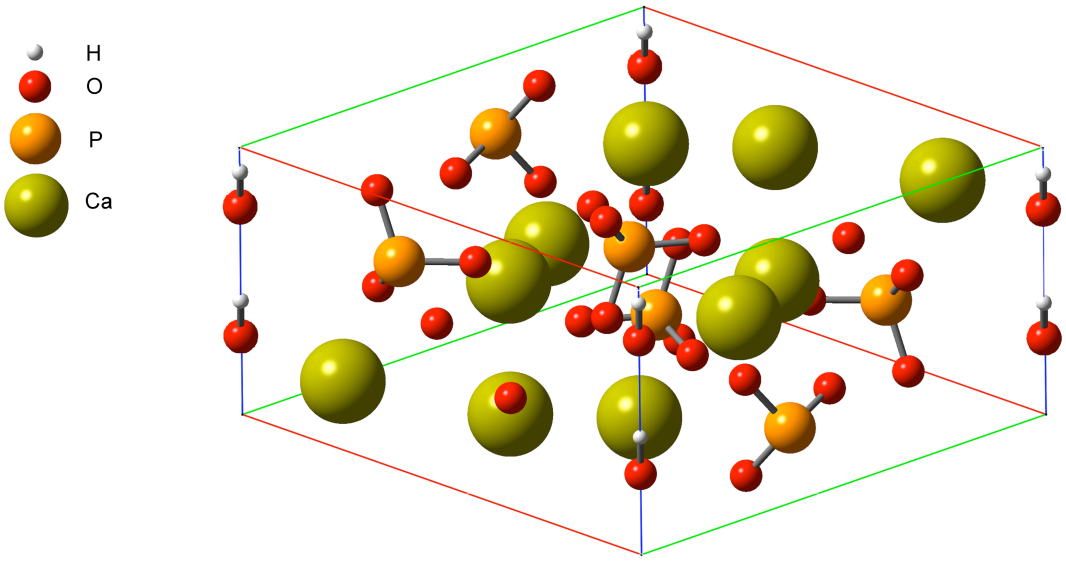

Figure 1. Schematic representation of HAP unit cell.

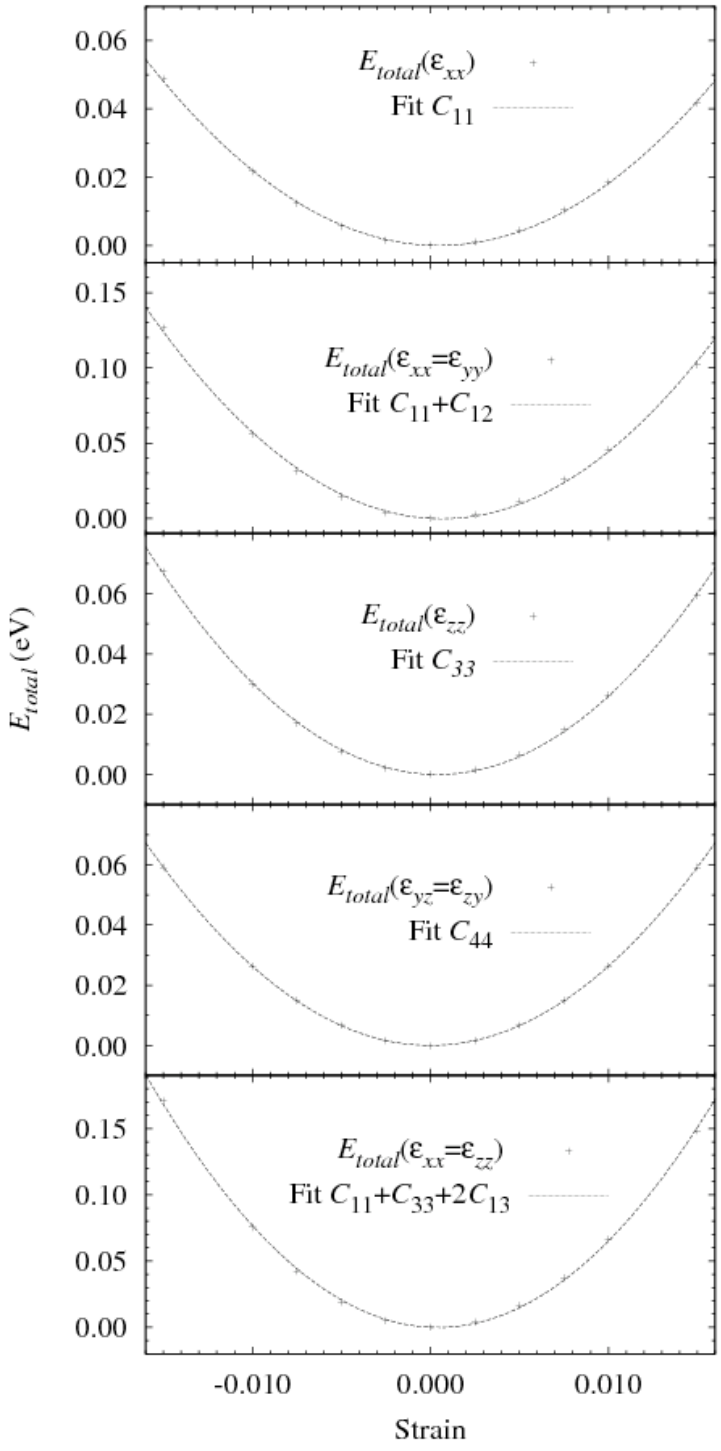

Figure 2. Ab initio energy vs strain data of HAP.